Return period of vegetation uprooting by flow

Citation for published version:
Calvani, G, Perona, P, Zen, S, Bau', V & Solari, L 2019, 'Return period of vegetation uprooting by flow', *Journal of Hydrology*, vol. 578, 124103. https://doi.org/10.1016/j.jhydrol.2019.124103

Digital Object Identifier (DOI):
10.1016/j.jhydrol.2019.124103

Link:
Link to publication record in Edinburgh Research Explorer

Document Version:
Peer reviewed version

Published In:
Journal of Hydrology

Return period of vegetation uprooting by flow

Giulio Calvani[a,b,*], Paolo Perona[b], Simone Zen[b], Valentina Bau'[b], Luca Solari[a]

[a] *Department of Civil and Environmental Engineering, School of Engineering, University of Florence, via S. Marta 2, 50139 Florence, Italy*
[b] *School of Engineering, Institute for Infrastructure and Environment, The University of Edinburgh, The King's Buildings, EH9 3FB Edinburgh, United Kingdom*

Abstract

Fluvial environments are dynamic systems whose evolution and management are strongly affected by the resilience of riparian vegetation to uprooting by flow. Similarly to other natural phenomena, the interactions between flow, sediment and vegetation uprooting is governed by both the magnitude and duration of hydrological events. In this work, we analytically derive the link between probabilities of plant uprooting by flow and the return time of corresponding hydrologic erosion events. This physically-based analysis allows to define the key parameters involved in the plant uprooting dynamics, and to link the uprooting probability of riparian vegetation to plant biomechanical characteristics, hydrological regime and sediment parameters. For example, we show how the rooting depth changes the return time of critical hydrologic event uprooting plants with different probabilities. The model also shows

*Corresponding author at: Department of Civil and Environmental Engineering, School of Engineering, University of Florence, via S. Marta 2, 50139 Florence, Italy
Email address: giulio.calvani@unifi.it (Giulio Calvani)

the difference between magnitude driven and duration driven flow uprooting events. The proposed approach is eventually validated against data from field measurements and numerical simulations of pioneer woody species for two flood events with different return period. Our approach demonstrates the strong interrelations between the hydrological river regime and vegetation properties and suggests that such interactions may be key for species recruitment and consequent ecosystem shifts when hydrological regime is altered by either human or climate changing scenarios.

Keywords: Peak Over Threshold, Poisson process, flow erosion, plant uprooting, type II uprooting

---

1. Introduction

Fluvial environments are dynamic systems whose evolution is governed by the interactions between vegetation dynamics, sediment processes and flow regime. Riparian plants alter turbulence structures, flow velocity and sediment transport (Nepf, 2012b). At the same time, the alternation of low and high flow discharges drives the recruitment, growth and decay of riparian vegetation (Edmaier et al., 2011). Particularly during high stage events, vegetation is subjected to drag force and plant removal occurs when root anchoring force is reduced through bed erosion to equal the drag (named uprooting Type II after (Edmaier et al., 2011)). Vegetation uprooting under flow and scour constraints (Type II) was investigated by Edmaier et al. (2015) in laboratory experiments with *Avena sativa* and by Bywater-Reyes et al. (2015) in field measurements. Calvani et al. (2019a) used flume experiments with *Avena sativa* and *Salix purpurea* and field measurements to test and validate a model able to predict the critical bed erosion depth for which uprooting occurs. All these studies agree that the amount of bed erosion leading to plant uprooting by flow is smaller than the initial rooting depth, thus supporting the critical rooting depth model (Edmaier et al., 2011; Calvani et al., 2019a). Perona and Crouzy (2018) hypothesized that for low plant size vs sediment size ratio, the critical rooting depth would correspond to a critical erosion depth. The latter is achieved by applying an erosion rate, which is the superposition of deterministic mean scouring (i.e., scouring happening over a characteristic longitudinal length scale) and random fluctuations mainly induced by turbulence and sediment transport mechanics.

Bed elevation changes, which include deposition and erosion, are regulated by the Exner equation, which states that time changing rate in bed elevation depends on the spatial variability of sediment fluxes. Specifically, in a river reach, erosion takes place when downstream sediment outflow is larger than the sediment inflow coming from upstream. Under a 1D framework, the corresponding mathematical formulation is the 1D-Exner equation,

$$\frac{\partial \eta(x,t)}{\partial t} = -\frac{1}{(1-\lambda_s)\ B}\frac{\partial Q_s}{\partial x} \tag{1}$$

where $\eta(x,t)$ is the bed elevation, x is the coordinate along the streamwise direction of the main channel, t is time, λ_s is the sediment porosity, B is the channel width and $Q_s(x,t)$ is the sediment discharge. At the time scale of a single flood event, the difference in sediment transport fluxes between two consecutive sections $\left(\Delta Q_s/\Delta x = \frac{1}{\Delta x}\int_1^2 dQ_s\right)$ is related to the bed shear stress acting at the bottom of the channel, which depends on the average flow velocity and, in turn, on the flow discharge. Therefore, the amount of erosion achieved during a flood event depends both on the magnitude and the duration of the event itself.

Flow discharge drives the uprooting process and, therefore, the hydrological time scale of flood events governs the recruitment of riparian vegetation species. Accordingly, riparian and aquatic species would have adapted their biomechanical properties in order to withstand the flow regime and increase survival chances during stress periods, due to either drought or flood events (Karrenberg et al., 2002; Gibling and Davies, 2012; Gurnell, 2014). As a result, the link between vegetation dynamics and hydromorphological time scales may represent the key factor to understand the biological evolution of riparian species and predict their effects on ecosystem dynamics (Calvani et al., 2019b). Such link was seldom investigated in literature, mostly by focusing on short time horizon only (Corenblit et al., 2015), although the interactions among native and invasive alien species and river morphodynamics employ decades to evolve (Habersack, 2000; Solari et al., 2016). To this purpose, an analysis on the long term (return period) is therefore sought, as well as the definition of an hydrograph associated to such return period. This is particularly required when both the magnitude and the duration of the flow event play a fundamental role in flow-time related processes, such as flood risk modelling and management (e.g., Mignot et al., 2018; Tanaka et al., 2017), dam overtopping (e.g., Schmocker and Hager, 2009) and sediment transport (e.g., Powell et al., 2001), among others.

In this work we link the uprooting probability P_τ to the extreme value analysis of a flow discharge Compound Poisson Process (CPP) using the Peak Over Threshold (POT) methodology. POT is a common mathematical approach to evaluate the occurrence probability (i.e., return period) of rare extreme events and is widely used in many disciplines, such as meteorology, geological, hydraulic and structural engineering and earth sciences (e.g., Leadbetter, 1991; Önöz and Bayazit, 2001; Novak, 2011; Castillo, 2012). We additionally provide a formulation for the statistically average hydrograph of a flow event associated to such threshold and its return period. We then apply the proposed formulation to the case study of vegetation removal by flow and bed erosion (Type II uprooting). We combine the POT of the CPP and the probabilistic model of plant removal to correlate the hydrological parameters to the return period of riparian vegetation uprooting probability. As last, we perform a sensitivity analysis on the parameters involved and test the proposed approach against field measurements data from Bywater-Reyes et al. (2015).

2. Methodology

2.1. The uprooting model

Consider figure 1, which represents the uprooting process investigated by Perona and Crouzy (2018). Scouring trajectories originate from the initial bed level ($\eta = 0$), reduce plant anchoring, until the critical erosion depth (i.e., $\eta = -L_e$) is achieved, then plant is uprooted. The different trajectories evolve according to the flow hydrograph $Q_\xi(t)$ and the stochasticity in the erosion process, g_t. Such process results in a probability distribution function, $p_\tau(t)$, of the times leading to uprooting. According to Perona and Crouzy (2018), the probability distribution function of time to uprooting, $p_\tau(t)$, reads:

$$p_\tau(t) = \frac{L_e}{2\sqrt{\pi\ G^3(t)}} \left(\frac{g_t(t)}{2}\ \mathrm{Exp}\left[-\ \frac{(L_e - V(t))^2}{4\ G(t)} \right] \right. \\ \left. + W(t)\ \mathrm{Exp}\left[\frac{L_e\ V(t)}{G(t)} \right] \right) \tag{2}$$

where L_e is the critical erosion depth for plant uprooting to occur, $g_t(t)$ describes the strength of uncorrelated Gaussian noise of the erosion process, $G(t) = \frac{1}{2}\int_0^t g_t(\tau)\ d\tau$, $V(t) = \int_0^t \dot{L}_d(\tau)\ d\tau$ and $W(t) = \sqrt{\pi\ G(t)}\ \mathrm{Erfc}\left[\frac{L_e + V(t)}{2\ \sqrt{G(t)}}\right]$ $\left(\dot{L}_d(t) - \frac{g_t(t)}{2}\ \frac{V(t)}{G(t)}\right)$, with τ the dummy time variable of integration. Therein, the deterministic part of the root exposing rate due to bed erosion is $\dot{L}_d = \dot{\eta}_d(t)\ dL/d\bar{\eta}$ where $dL/d\bar{\eta}$ accounts for the root shape and architecture within the soil. We assume $dL/d\bar{\eta} = 1$ under the simplifying hypothesis of root vertical development (Edmaier et al., 2015; Calvani et al., 2019a). This requires that the average hydrograph of an event must be defined in order to calculate the associated erosion rate, its total duration $\hat{T}_\xi$ (figure 1) and the correspondent uprooting probability $P_\tau(t = \hat{T}_\xi)$.

The quantity g_t has the unit of a diffusivity (i.e., $\mathrm{m}^2\,\mathrm{s}^{-1}$) and models the stochasticity of turbulence and sediment transport mechanics. Since no formulation are available in literature, we argue that a relationship for the quantity g_t can be sought in the formula of the eddy viscosity (Pope, 2001; Michael, 2015), as disturbances in sediment transport are directly related to fluid obstacle interactions and flow turbulence at the stem scale (Nepf, 2012a; Perona and Crouzy, 2018). Thus, the formula reads:

$$g_t(t) = l_s \cdot u_* \tag{3}$$

where l_s is the *sediment mixing length* (i.e., a length scale along the vertical direction y) and u_* is the shear velocity, that plays the role of a velocity scale along the longitudinal direction x, similarly to the case of eddy viscosity ν_t. We set the sediment mixing length l_s equal to the mobilized sediment layer thickness, which is in the order of magnitude of the D_{90}. Accordingly, the equation for l_s reads

$$l_s = k_g \cdot D_{90} \tag{4}$$

where k_g is a multiplying coefficient equal to 2, according to Parker (1990). For the sake of dimensional consistency in unit of measurement, a multiplying constant equal to $1\,\mathrm{s\,d^{-1}}$ has to be taken into account when considering the strength of the Wiener process (see Eq. (2.10) in Perona and Crouzy (2018)).

Finally, the relationship for the probability of Type II uprooting $P_\tau(t)$

reads (Perona and Crouzy, 2018):

$$P_\tau(t) = \int_0^t p_\tau(\tau)\ d\tau \tag{5}$$

2.2. Peak Over Threshold analysis

We now approximate the flow discharge signal to a Compound Poisson Process. The Compound Poisson Process (CPP) is a common mathematical representation to describe the dynamics of stochastic systems where instantaneous perturbations cause sudden jumps in the state variable (Cox and Miller, 1965; Ridolfi et al., 2011). Forest fire spread (Daly and Porporato, 2006; Zen et al., 2018), avalanches induced by snowfall (Perona et al., 2007, 2012), groundwater recharge, soil moisture increase (Rodriguez-Iturbe et al., 1999; Botter et al., 2007), river flood events due to heavy rainfall (Todorovic, 1978; Önöz and Bayazit, 2001; Lague, 2010) and ecomorphodynamics (Crouzy and Perona, 2012; Bertagni et al., 2018) are only some of the natural processes that can be modelled using the CPP approach. In the following, we focus on flow discharges in a straight channel, characterized by constant width and bed slope. We assume flow discharge $q(t)$ being driven by a deterministic drift (i.e., exponential decrease $\mathrm{Exp}[-t/\tau_P]$, with decay rate τ_P)

and instantaneous random positive jumps (with average frequency λ_P) representing the flood events (figure 2) (Botter et al., 2007). The average flow discharge μ_P of the CPP is $\mu_P = \gamma_P \cdot \lambda_P \cdot \tau_P$, where γ_P is the mean values of the jumps. Accordingly, flow discharge can be modelled by a probabilistic distribution function, $p(q)$ (figure 2), of the form (Lague et al., 2005; Botter et al., 2007):

$$p(q) = \frac{1}{q\,\Gamma(\beta_P)}\ \mathrm{Exp}\left[-\frac{q}{\gamma_P}\right]\ \left(\frac{q}{\gamma_P}\right)^{\beta_P} \tag{6}$$

where $\Gamma[\beta_P]$ is the complete Gamma function (Abramowitz and Stegun, 1965) with $\beta_P = \lambda_P \tau_P$.

Next, we perform an extreme value analysis using the Peak Over Threshold (POT) approach developed by Todorovic (1970) and then applied to exponentially distributed peak events (CPP) by Zelenhasic (1970) and Önöz and Bayazit (2001), among others. Once a certain threshold ξ is set, POT allows to evaluate the return period $T(\xi)$ of the flow discharge higher than such threshold. For the sake of brevity, only the main results are reported here below, whereas we address the reader to Calvani (2019) for the calculation steps. The return period $T(\xi)$ simply reads:

$$T(\xi) = \frac{1}{1 - P_\xi} \tag{7}$$

Therein, the probability of events higher than the threshold ξ, P_ξ as given by the POT analysis, is equal to:

$$P_\xi = \mathrm{e}^{-T\ \lambda'_P\ P_\xi^+} \tag{8}$$

where T is a temporal quantity set equal to 1d for the aim of the POT, $\lambda'_P = \frac{\mathrm{e}^{-\phi}\phi^{\beta_P}}{\tau_P\Gamma[\beta_P]}$ is the average frequency of upcrossing the threshold ξ; ϕ is the ratio between the threshold ξ and the mean value of pulses γ_P; P_ξ^+ is the probability of the signal $q(t)$ (figure 2) to be higher than the threshold ξ, that is $P_\xi^+ = \int_\xi^\infty p(q)dq = \frac{\Gamma[\beta_P,\phi]}{\Gamma[\beta_P]}$ (Ridolfi et al., 2011) where $\Gamma[\beta_P, \phi]$ is the upper incomplete Gamma function (Abramowitz and Stegun, 1965). It must be clear that the two frequencies, λ_P and λ'_P, represent different quantities for the CPP. The first one, λ_P, is a property of the process and depends, in this case, on the hydrological regime of the river, only. On the contrary, the second one, λ'_P, depends on the threshold value, ξ. To clarify this point, one can compare the whole number of jumps in figure 2 (which depends on λ_P) to the number of jumps across above the threshold ξ (which depends on λ'_P).

2.3. Reference mean event

For a given threshold ξ and its return period $T(\xi)$ (Eq. (7)), we calculate the associated reference mean event, which represents a statistically averaged flow hydrograph following a jump (peak) above the threshold ξ and lasts until downcrossing the threshold Q_{cr}. As we focus on events able to uproot vegetation after riverbed erosion (i.e., Type II uprooting), we consider flow discharge above the threshold value for incipient motion of sediment Q_{cr} only, which we assume equal to the one for the incipient erosion. Such value can be calculated as follows:

$$Q_{cr} = {\tau_{cr}^{*}}^{5/3} \left(\frac{\rho_s - \rho}{\rho}\right)^{5/3} D_{50}^{5/3} \ \frac{B}{n} \ S^{-7/6} \tag{9}$$

where τ_{cr}^{*} is the critical Shields parameter equal to either 0.03, according to Parker et al. (2007) for gravel bed rivers subjected to bedload transport, or τ_{SL}^{*} for sand-bed rivers with suspended load; ρ_s and ρ are sediment and water density, respectively; D_{50} is the mean grain size; B is the river width; n is the Manning coefficient and S is the bed slope. The critical Shields parameter for sand-bed rivers τ_{SL}^{*} can be calculated using Brownlie's equation (Brownlie, 1981).

We address the reader to Calvani (2019) for the whole mathematical approach and report here the final equation of the reference mean event $Q_\xi(t)$ defined by a piecewise function:

$$Q_\xi(t) = \begin{cases} Q_0(\xi)\ \mathrm{e}^{-t/\tau_1} & \left[0 \le t \le T_\xi^{+}\right] \\ \xi\ \mathrm{e}^{-(t-T_\xi^{+})/\tau_2} & \left[T_\xi^{+} < t \le \hat{T}_\xi\right] \end{cases} \tag{10}$$

Quantities $Q_0(\xi)$, τ_1 and τ_2 are calculated according to the properties of the Compound Poisson Process: particularly, the average time, T_ξ^+, and the average flow value, $\bar{Q}_{q>\xi}$, above the threshold ξ, and the average time, $T_{\xi \to Q_{cr}}$, from the threshold ξ to the threshold Q_{cr}. The temporal quantities, T_ξ^+ and $T_{\xi \to Q_{cr}}$, are related to the concept of mean first passage time, that is the average time that a signal upcrosses or downcrosses a certain threshold value (Laio et al., 2001; Ridolfi et al., 2011). The total duration of the reference mean event is, therefore:

$$\hat{T}_\xi = T_\xi^+ + T_{\xi \to Q_{cr}} \tag{11}$$

To this regard, we must point out that flow volume conservation is exactly satisfied for the first part of the reference mean event only (i.e., from Q_0 to ξ), as this is imposed using the conditions for T_ξ^+ and $\bar{Q}_{q>\xi}$. The second exponential decay (i.e., from ξ to Q_{cr}) is calculated using the exact formulation for the average time $T_{\xi \to Q_{cr}}$. This may lead to error in the flow volume conservation, and the outcomes of this assumption will be explored in Section 3.1.

2.4. Erosion rate

In order to account for bed elevation changes and scouring events promoting Type II uprooting during high flow events, we couple the time-varying flow discharge to the 1D Exner (Eq. (1)) and sediment transport relationships. For the sediment transport, we consider both the cases of bed and suspended load. Specifically, we assume a Meyer-Peter-Müller type formula (Wong and Parker, 2006) for bedload and the van Rijn's model (van Rijn, 1984) for the suspended load. For the resultant relationships to be as simple as possible, we neglect the effects of the time derivative in the momentum equation at the time scale of the process. As a result, bed shear stress τ_b and water depth Y can be calculated from flow discharge only, by knowing channel geometry and involving the Manning relation for normal flow. Additionally, for the channel geometry, we assume a wide rectangular cross-section with constant width and bed slope. By combining the aforementioned formulas and assuming negligible upstream sediment discharge (Perona and Crouzy, 2018), we obtain a relationship for the net (deterministic) erosion rate $\dot{\eta}_d$ where the typical structure of sediment transport formula above critical threshold and exponent 3/5 coming from Manning relation can be recognized. The relation reads:

$$\dot{\eta}_d\,(t) = \psi_1\ \psi_2\ \left(q^{\frac{3}{5}}(t) - Q_{cr}^{\frac{3}{5}}\right)^b \cdot \left(q^{\frac{3}{10}}(t)\ \cdot\ I(q(t), D_{50})\right)^{a_{ST}} \tag{12}$$

where ψ_1 is a coefficient depending on physical parameters, river size and sediment properties, ψ_2 is a coefficient depending on the main type of sediment load, b is the exponent in the sediment transport formula (e.g., $^3/_2$ in the case of van Rijn's and MPM's models), $I(q(t), D_{50})$ is a quantity given by the Einstein's integrals (Einstein, 1950) and depending on mean grain size D_{50} and flow discharge in the case of suspended load only, and a_{ST} is a parameter equal to either 0 for bedload or 1 for suspended load. The relation for the parameter ψ_1 reads:

$$\psi_1 = \frac{\sqrt{g}\ D_{50}^{1-b}}{(1-\lambda_s)\Delta x}\ \left(\frac{\rho_s - \rho}{\rho}\right)^{-b}\ \left(\frac{n}{B}\right)^{\frac{3}{5}b}\ S^{\frac{7}{10}b} \tag{13}$$

where g is the acceleration due to gravity, λ_s is the sediment porosity, Δx is the length scale along the streamwise direction where the spatial derivative of sediment transport (right-hand side term in Eq. (1)) can be approximated by the finite difference. Following the approximation suggested by Perona and Crouzy (2018), Δx is the spatial scale, where net (parallel) bed erosion takes place. The coefficient ψ_2 depends on the main type of sediment transport, according to the following relation:

$$\psi_2 = \begin{cases} \alpha_{BL}\ D_{50}^{1/2}\ \left(\frac{\rho_s-\rho}{\rho}\right)^{\frac{1}{2}} & a_{ST}=0 \\ \alpha_{SL}\ \left(\frac{n}{B}\right)^{\frac{3}{10}} S^{\frac{7}{20}}\ R_{ep}^{\frac{-2}{10}}\ {\tau_{SL}^{*}}^{b} & a_{ST}=1 \end{cases} \tag{14}$$

Therein, α_{BL} is the coefficient in the bedload formula (e.g., 3.97 in Wong and Parker (2006)), $\alpha_{SL} = 0.174$ is the coefficient in van Rijn's formula for suspended load (van Rijn, 1984) and R_{ep} is the particle Reynolds number. It is worth to mention that, in the case of bedload (α_{ST}=0 in Eq. (14)), when b=1.5 (e.g., Meyer-Peter and Müller, 1948; Wong and Parker, 2006), the mean grain size D_{50} cancels out in the product $\psi_1 \cdot \psi_2$ in Eq. (12). As a result, the erosion rate $\dot{\eta}_d(t)$ depends on the mean grain size, D_{50}, by the critical flow for incipient motion of sediment, Q_{cr} (Eq. (9)), only.

3. Results

3.1. Reference mean event

A graphical explanation of the reference mean event $Q_\xi(t)$ (Eq. (10)) is reported in figure 3a), with the associated erosion rates due to bedload and suspended load and the critical thresholds, Q_{cr}, for incipient sediment transport (Eq. (9)). Figure 3b) shows the comparison between a reference mean event (blue line) and some Compound Poisson Process events (thin black lines) between the two thresholds ξ and Q_{cr}.

Due to assumptions made in the calculations of the reference event (Eq. (10)), particularly the second exponential decay from ξ to Q_{cr} (Section 2.3), we compared the flow volume of the reference mean event $\left(\text{i.e., } \int_0^{\hat{T}_\xi} Q_\xi(t)dt\right)$ to the average flow volume of some events taken from a CPP, according to various combinations of the parameters λ_P and τ_P, and with respect to different values of the threshold ξ. The comparison was carried out for two ideal rivers characterized by different hydro-morphological parameters. The first one, here named the *Small River*, has a cross section width, B, equal to 50m, bed slope, S, equal to 0.005, and grain size distribution characterized by D_{50} equal to 0.1m and D_{90} equal to 0.15m. The corresponding hydrology is characterized by a mean flow discharge, μ_P, equal to $15\text{m}^3\,\text{s}^{-1}$, average frequency of events, λ_P, equal to 0.1d^{-1}, and exponential decay rate, τ_P, equal to 1.5d. The second river, here named the *Large River*, has a cross section width, B, equal to 100m, bed slope, S, equal to 0.002, and grain size distribution characterized by D_{50} equal to 0.04m and D_{90} equal to 0.1m. The corresponding hydrology is characterized by a mean flow discharge, μ_P, equal to $400\text{m}^3\,\text{s}^{-1}$, average frequency of events, λ_P, equal to 0.1d^{-1}, and exponential decay rate, τ_P, equal to 1.5d. For both the rivers, the D_{90} was used to calculate the Manning coefficient n, according to the empirical relation $n = D_{90}^{1/6}/26$. The results of the comparison are shown in figure 4.

The comparison shows that, as expected, the formulation of the reference mean event (Eq. (10)) does not capture exactly the average flow volume during the exponential decay from the upper threshold ξ to the lower threshold Q_{cr}. Nevertheless, the agreement seems satisfactorily as the relative error is overall less than 5%, with a maximum of 15% for some very particular combinations of the parameters λ_P and τ_P (e.g., λ_P=0.02d^{-1} and τ_P=7d) which are uncommon in natural rivers. It is worth to note that the flow volume calculated using the reference mean event overestimates the numerical data for most of the λ_P-τ_P combinations in the Small River. On the contrary, it has the tendency to underestimate the numerical data in the Large River. As a result, the formulation of the reference mean event yields to predicting errors in the uprooting probability. To this regard, we compared the average uprooting probability of fifty events taken from a CPP with two different values of the higher threshold ξ for the Small River and the Large River (figure 3c,d). For the Small River, for the first value of the threshold, ξ=125m^3 s^{-1}, the average uprooting probability of the CPP events was P_τ=0.24, whereas the uprooting probability calculated using the corresponding reference mean event was $P_\tau(t = \hat{T}_\xi)$=0.32. For the second threshold value, ξ=180m^3 s^{-1} (figure 3c), the uprooting probability from the CPP was P_τ=0.24, whereas $P_\tau(t = \hat{T}_\xi)$=0.56. For the Large River, the first threshold value was set to ξ=550m^3 s^{-1} and the uprooting probability of the CPP events was P_τ=0.53, with the corresponding $P_\tau(t = \hat{T}_\xi)$ of the reference mean event equal to 0.54 (figure 3d). For the second value of the threshold, ξ=750m^3 s^{-1}, the uprooting probabilities were P_τ=0.58 and $P_\tau(t = \hat{T}_\xi)$=0.55. As a consequence of the approximation of the flow volume (figure 4), the approach leads to slight underestimations of the uprooting probability in the case of the Large River and overestimations in the case of the Small River. Therefore, we are confident that the case of ξ=550m^3 s^{-1} in the Large River with slight overestimation of the uprooting probability depends on the particular randomly chosen events that are mainly lying below the reference mean event (see figure 3d).

3.2. Resilience to vegetation uprooting

We performed the calculations of $P_\tau(t = \hat{T}_\xi)$ for both the rivers presented in the previous section, in the case ofbedload transport (i.e., α_{ST}=0 in Eq. (14)). For the sake of simplicity, we did not consider the case of suspended load (i.e., α_{ST}=1 in Eq. (14)), even when the Shields number would be large enough to support its occurrence at high value of the flow discharge. The length scale, Δx in Eq. (13), was set equal to $6{\cdot}B$, which is roughly the length scale of potential river bars (Leopold and Wolman, 1957). Due to the highly non-linear relationships involved in the calculation of the uprooting probability $P_\tau(t = \hat{T}_\xi)$, we performed a graphical analysis on the effects of varying parameter values, one at a time. In particular, we considered the effects of the critical erosion for uprooting, L_e and the coefficient α_{BL} in bed load sediment transport formula, by accounting for constant values of the hydrological parameters, μ_P, λ_P and τ_P. Additionally, we kept constant the fluctuations of the sediment transport rate (g_t=0.05m^2 d^{-1}), regardless of Eq. (3), to highlight the changes induced by varying the tested parameter. Figure 5 shows the trend of the uprooting probability function, $P_\tau(t = \hat{T}_\xi)$, versus the corresponding return period T_ξ at varying the parameters, for the Small River and the Large River, respectively.

For both rivers, the critical erosion depth L_e plays an important role in the probability of uprooting. In case of the Small River, figure 5a) shows that an increment of 0.25m in L_e (e.g., from 0.5m to 0.75m) raises survival chances (=1-P_τ) by more than 30% for a yearly flow event. For the Large River (figure 5c), the same consideration implies an increment of 20% in the survival chances. According to Calvani et al. (2019a), plants do not need to grow root as deep as that amount, as soil strength increases with depth. Furthermore, the same gain in L_e can be achieved by reducing the frontal area subjected to drag, either by increasing flexibility (i.e., reconfiguration) or by physically losing leaves. The latter mechanism appears to be a possible strategy for riparian plants in the temperate zone to adapt their deciduous period to autumn and winter seasons, not only to save energy, but also to withstand the larger and more frequent peak events.

For the effects of the coefficient of the bedload transport formula, we considered the original value proposed by Wong and Parker (2006) and four other values, differing by ±25% and ±50%. For the Large River, figure 5d) shows that increasing the coefficient α_{BL} by 25% raises theuprooting probability by roughly 5% in the whole range of the tested return periods. A similar behaviour in the function P_τ can be observed when the coefficient α_{BL} decreases by 25% (α_{BL}=2.978). In this case we observed a decrease in the uprooting probability by 5%, only. As a result, the parameter α_{BL} in the range of tested values does not seem to significantly affect the uprooting probability. Different results were obtained for the Small River, where the variation imposed in the bedload transport coefficient, α_{BL}, affect the uprooting probability by more than 10% for a yearly flow event (figure 5b). Particularly, for the case of doubling the bedload transport coefficient, the uprooting probability increases by 25%.

Additionally, we investigated the effects of varying the hydrological parameters, specifically the average jump value γ_P, the average frequency of jumps λ_P, and the exponential decay rate τ_P, and the grain size distribution, with particular focus on the mean grain size D_{50}. The results of the analysis are reported in figures 6 and 7, for the Small River and the Large River, respectively.

Both rivers show similar trends of the uprooting probability, while varying the same parameter. Similarly to the case with constant mean flow discharge μ_P (figure 5), the influence of the investigated parameters is more evident in the Small River, when compared to the Large River. Such result is particularly clear in figures 6 and 7 when comparing panels c), varying the mean value of jump, γ_P, and panels d), at varying the mean grain size D_{50}.

Consider now, the case of figure 8, where the uprooting probabilities of two different cross sections in the same river are shown. Hydro-morphological parameters are representative of the Thur River (CH), at the two measuring stations of Jonschwil, Mühlau (upstream) and Andelfingen (downstream).

Data are reported within the figure. The uprooting probability $P_\tau(t = \hat{T}_\xi)$, for the same critical erosion length (L_e=0.75m) and erosion process noise (g_t=0.05m^2 d^{-1}), shows the existence of a return period for which the two curves intersect. Such return period corresponds to equal uprooting probability in both the cross sections, thus supporting the idea of selecting the survival of equal vegetation species along the whole river reach. We explain this trend by considering the different reference mean events and the associated p_τ obtained for the tow different cross sections. For low return periods (e.g., $T(\xi)$ ≈0.3y), the uprooting probability is higher in the downstream cross section (DS). The main reason is the longer duration of the reference mean event for the DS cross section, if compared to that in the upstream (US) one (i.e., $\hat{T}_\xi^{DS} > \hat{T}_\xi^{US}$). On the contrary, for higher return periods (e.g., $T(\xi)$ ≈10y), the uprooting probability is higher in the US cross section. Although the condition $\hat{T}_\xi^{DS} > \hat{T}_\xi^{US}$ still applies, the probability distribution function, p_τ, in case of the US cross section (see bottom-left inset panel in figure 8) shows a very remarkable peak, leading to a higher integral value, P_τ. We refer to this dualism as *duration driven* and *magnitude driven* uprooting events, respectively.

3.3. Real case application

We applied the proposed methodology and the uprooting model to the case study of the Santa Maria River (Arizona, USA). This river was investigated by Bywater-Reyes et al. (2015) and plants on a bar along it were mechanically uprooted under different conditions of scouring. As a results, data of flow discharge to fit the CPP and measurements of root resistance and plant geometry are both available.

Figure 9a) shows the reference mean event and its associated erosion rate $\dot{\eta}$ driven by suspended load (a_{ST}=1 in Eq. (12)) for the 10y return period peak event. We calculated the uprooting probability according to different critical erosion length L_e and compared the results for the two flow discharges investigated by Bywater-Reyes et al. (2015) (Q_2=80m^3 s^{-1}; Q_{10}=460m^3 s^{-1}) and the plants uprooted under 0.30m scouring condition. For the measured plants, we calculated the minimum, median and maximum of uprooting probability of according to the corresponding velocities as output numerical simulation carried out by Bywater-Reyes et al. (2015) for the two investigated return periods. Figure 9b) shows the uprooting probability $P_\tau(t = \hat{T}_\xi)$ versus the threshold ξ for different values of the unknown variable L_e for the Santa Maria River. The critical erosion length $L_e = 0.33$m used in figure 9b) was calculated according to the model proposed by Calvani et al. (2019a) for the mechanically uprooted plants for which measurements of intact root (i.e., main root length) were available. Uprooting probability for measured plants are shown as boxplots. As a final result of our analysis, we found a very good agreement between measured and modelled uprooting probability for both the flow discharges. Therefore, this supports the validity of our analysis and the robustness of our approach.

4. Discussion

For the sake of clarity, we have considered the reference mean event $Q_\xi(t)$ starting when a jump in the Compound Poisson Process up-crosses the threshold ξ. This is replicated in the reference mean event by the initial jump from the critical value Q_{cr} to the the flow discharge $Q_0(\xi)$. This assumption is often legitimated by the generally shorter duration of the raising limb compared to that of the falling limb in a flow hydrograph. However, such hypothesis can not be satisfied in case of high correlated signals, for instance when the temporal scale τ_P governing the exponential decrease (deterministic drift in the CPP) is larger than the average interval between shots (i.e., λ_P^{-1}). In this case, a more appropriate formulation for the raising limb of the reference mean event must be provided. This is object of ongoing investigations. Nevertheless, hydrological regimes with such characteristics are uncommon so we are confident that the proposed formulation and methodology can be satisfactorily applied to most rivers (e.g., figure 9).

Additionally, in this section, we focused on Eq. (3) and the associated time-varying g_t. We investigated the effects of different values of k_g (Eq. (4)), representing the variability of the mobilized sediment layer thickness. We compared the resulting uprooting probabilities with constant and time-varying g_t. For the sake of the analysis, we consider the constant g_t as the integral average of the time-varying one over the entire duration $\hat{T}_\xi$ of the reference mean event $Q_\xi(t)$ for a given return period $T(\xi)$.

Figure 10 shows the comparison among uprooting probabilities with constant and time-varying g_t according to different values of k_g. Time-varying g_t plays a significant role in modifying the resultant $P_\tau(t = \hat{T}_\xi)$ only for either very high or very low values of k_g (e.g., $k_g = 0.2$ or $k_g = 20$). For more reasonable values (e.g., $k_g = 2$ (Parker, 1990)), the uprooting probabilities are very similar and, therefore, the average value defines the entire trend. This behaviour is clearly explained by the corresponding probability distribution functions, p_τ, plotted in the inset panels of figure 10 for two different return periods, $T(\xi)$. Moreover, for values of k_g equal to 4, time-varying g_t increases the uprooting probability for low return periods (e.g., $T(\xi)$ <11y), whereas $P_\tau(t = \hat{T}_\xi)$ is almost equal for slightly higher recurrence intervals (e.g., 10y $< T(\xi)$ <50y). For higher return period ($T(\xi)$ >50y), the uprooting probability with the time-varying g_t is lower than the correspondent with constant g_t. For even higher values ($k_g = 20$), the uprooting probability with time-varying g_t is always larger, for the tested range of return period and hydrological parameters. It is interesting to highlight that for k_g lower than 4, the uprooting probability function behaves in the opposite way. We didn't investigate on the threshold value of k_g that switches between the two different trends.

5. Conclusions

In this work, we linked the uprooting probability given by the stochastic model of Perona and Crouzy (2018) to the return period of flood events, calculated using the Peak Over Threshold method on a Compound Poisson Process. We proposed a simple approach to calculate a reference mean event for a given return period and its application to the stochastic model for the uprooting probability.

Our analysis has been carried out for one single event and returns the probability of uprooting associated to characteristic flood/erosion events of assigned return period. However, riparian vegetation may withstand many more erosion events during its life. This suggests that the interval between consecutive peak events and the ability for riparian species to recover and grow in this interval play a fundamental role in the evolution of water driven patterns (Bertagni et al., 2018), both from the biological and the morphological point of view (Edmaier et al., 2015; Perona and Crouzy, 2018; Calvani et al., 2019b). For this reason, the role of the intertime between consecutive flood events and their cumulative effects should be further investigated.

Our results suggest that the critical erosion depth L_e and average frequency of peak events λ_P are the key parameters to define the uprooting probability of riparian vegetation in a given river basin. Yet, this study confirms that long time scale interactions between river hydro-morphology and riparian vegetation are fundamental to shape the riverine environment (Bywater-Reyes et al., 2015). For a given hydrological regime, the mechanisms at the base of such interactions may be key to select species according to their ability to survive in water-driven environments. For instance, invasive riparian plants can take advantage of these interactions, leading to colonization of new fluvial landforms and suppression of local species, due to alteration in the hydrological regime by either human impacts (Tealdi et al., 2011; Coletti et al., 2017) or climate change (Serrat-Capdevila et al., 2007; House et al., 2016).

Acknowledgments

This work was performed while the author was visiting the Chair of Environmental Engineering at the School of engineering of the University of Edinburgh, which is therefore deeply acknowledged. We thank Editors and two anonymous Reviewers for comments and suggestions that greatly improved the manuscript.

References

Abramowitz, M., Stegun, I.A., 1965. Handbook of mathematical functions: with formulas, graphs, and mathematical tables. volume 55. Courier Corporation.

Bertagni, M.B., Perona, P., Camporeale, C., 2018. Parametric transitions between bare and vegetated states in water-driven patterns. Proceedings of the National Academy of Sciences 115, 8125–8130.

Botter, G., Porporato, A., Daly, E., Rodriguez-Iturbe, I., Rinaldo, A., 2007. Probabilistic characterization of base flows in river basins: Roles of soil, vegetation, and geomorphology. Water Resources Research 43.

Brownlie, W.R., 1981. Prediction of flow depth and sediment discharge in open channels. Technical Report No. KH-R-43A. Keck Laboratory, California Institute of Technology.

Bywater-Reyes, S., Wilcox, A.C., Stella, J.C., Lightbody, A.F., 2015. Flow and scour constraints on uprooting of pioneer woody seedlings. Water Resources Research 51, 9190–9206.

Calvani, G., 2019. Riparian vegetation in fluvial environments: linking timescales through flow uprooting. Ph.D. thesis. University of Florence. Florence (IT).

Calvani, G., Francalanci, S., Solari, L., 2019a. A physical model for the uprooting of flexible vegetation on river bars. Journal of Geophysical Research: Earth Surface 124, 1018–1034. doi:10.1029/2018JF004747.

Calvani, G., Perona, P., Schick, C., Solari, L., 2019b. Biomorphological scaling laws from convectively accelerated streams. Earth Surface Processes and Landforms Under peer review.

Castillo, E., 2012. Extreme value theory in engineering. Elsevier.

Coletti, J.Z., Vogwill, R., Hipsey, M.R., 2017. Water management can reinforce plant competition in salt-affected semi-arid wetlands. Journal of hydrology 552, 121–140.

Corenblit, D., Baas, A., Balke, T., Bouma, T., Fromard, F., Garófano-Gómez, V., González, E., Gurnell, A.M., Hortobágyi, B., Julien, F., et al., 2015. Engineer pioneer plants respond to and affect geomorphic constraints similarly along water-terrestrial interfaces world-wide. Global Ecology and Biogeography 24, 1363–1376.

Cox, D., Miller, H., 1965. The theory of stochastic processes. Methuen, London (UK).

Crouzy, B., Perona, P., 2012. Biomass selection by floods and related timescales. part 2: Stochastic modeling. Advances in Water Resources 39, 97–105.

Daly, E., Porporato, A., 2006. State-dependent fire models and related renewal processes. Physical Review E 74, 041112.

Edmaier, K., Burlando, P., Perona, P., 2011. Mechanisms of vegetation uprooting by flow in alluvial non-cohesive sediment. Hydrology and Earth System Sciences 15, 1615–1627.

Edmaier, K., Crouzy, B., Perona, P., 2015. Experimental characterization of vegetation uprooting by flow. Journal of Geophysical Research: Biogeosciences 120, 1812–1824.

Einstein, H.A., 1950. The bed-load function for sediment transportation in open channel flows. Technical Report No. 1026, United States Department of Agriculture, Soil Conservation Service: Washington, DC.

Gibling, M.R., Davies, N.S., 2012. Palaeozoic landscapes shaped by plant evolution. Nature Geoscience 5, 99.

Gurnell, A., 2014. Plants as river system engineers. Earth Surface Processes and Landforms 39, 4–25.

Habersack, H.M., 2000. The river-scaling concept (RSC): a basis for ecological assessments, in: Assessing the Ecological Integrity of Running Waters. Springer, pp. 49–60.

House, A., Thompson, J., Acreman, M., 2016. Projecting impacts of climate change on hydrological conditions and biotic responses in a chalk valley riparian wetland. Journal of Hydrology 534, 178–192.

Karrenberg, S., Edwards, P., Kollmann, J., 2002. The life history of Salicaceae living in the active zone of floodplains. Freshwater Biology 47, 733–748.

Lague, D., 2010. Reduction of long-term bedrock incision efficiency by short-term alluvial cover intermittency. Journal of Geophysical Research: Earth Surface 115.

Lague, D., Hovius, N., Davy, P., 2005. Discharge, discharge variability, and the bedrock channel profile. Journal of Geophysical Research: Earth Surface 110.

Laio, F., Porporato, A., Ridolfi, L., Rodriguez-Iturbe, I., 2001. Mean first passage times of processes driven by white shot noise. Physical Review E 63, 036105.

Leadbetter, M.R., 1991. On a basis for 'Peaks over Threshold' modeling. Statistics & Probability Letters 12, 357–362.

Leopold, L.B., Wolman, M.G., 1957. River channel patterns: braided, meandering, and straight. US Government Printing Office.

Meyer-Peter, E., Müller, R., 1948. Formulas for bed-load transport, in: IAHSR 2nd meeting, Stockholm, appendix 2, IAHR. pp. 39–64.

Michael, L., 2015. Statistical turbulence modelling for fluid dynamics-demystified: an introductory text for graduate engineering students. World Scientific.

Mignot, E., Li, X., Dewals, B., 2018. Experimental modelling of urban flooding: A review. Journal of hydrology .

Nepf, H.M., 2012a. Flow and transport in regions with aquatic vegetation. Annual review of fluid mechanics 44, 123–142.

Nepf, H.M., 2012b. Hydrodynamics of vegetated channels. Journal of Hydraulic Research 50, 262–279.

Novak, S.Y., 2011. Extreme value methods with applications to finance. CRC Press.

Önöz, B., Bayazit, M., 2001. Effect of the occurrence process of the peaks over threshold on the flood estimates. Journal of hydrology 244, 86–96.

Parker, G., 1990. Surface-based bedload transport relation for gravel rivers. Journal of hydraulic research 28, 417–436.

Parker, G., Wilcock, P.R., Paola, C., Dietrich, W.E., Pitlick, J., 2007. Physical basis for quasi-universal relations describing bankfull hydraulic geometry of single-thread gravel bed rivers. Journal of Geophysical Research: Earth Surface 112.

Perona, P., Crouzy, B., 2018. Resilience of riverbed vegetation to uprooting by flow. Proc. R. Soc. A 474.

Perona, P., Daly, E., Crouzy, B., Porporato, A., 2012. Stochastic dynamics of snow avalanche occurrence by superposition of Poisson processes. Proc. R. Soc. A , rspa20120396.

Perona, P., Porporato, A., Ridolfi, L., 2007. A stochastic process for the interannual snow storage and melting dynamics. Journal of Geophysical Research: Atmospheres 112.

Pope, S.B., 2001. Turbulent flows. IOP Publishing.

Powell, D.M., Reid, I., Laronne, J.B., 2001. Evolution of bed load grain size distribution with increasing flow strength and the effect of flow duration on the caliber of bed load sediment yield in ephemeral gravel bed rivers. Water Resources Research 37, 1463–1474.

Ridolfi, L., D'Odorico, P., Laio, F., 2011. Noise-induced phenomena in the environmental sciences. Cambridge University Press.

van Rijn, L.C., 1984. Sediment transport, part II: suspended load transport. Journal of hydraulic engineering 110, 1613–1641.

Rodriguez-Iturbe, I., Porporato, A., Ridolfi, L., Isham, V., Coxi, D., 1999. Probabilistic modelling of water balance at a point: the role of climate, soil and vegetation, in: Proceedings of the Royal Society of London A: Mathematical, Physical and Engineering Sciences, The Royal Society. pp. 3789–3805.

Schmocker, L., Hager, W.H., 2009. Modelling dike breaching due to overtopping. Journal of Hydraulic Research 47, 585–597.

Serrat-Capdevila, A., Valdés, J.B., Pérez, J.G., Baird, K., Mata, L.J., Maddock III, T., 2007. Modeling climate change impacts–and uncertainty–on the hydrology of a riparian system: The san pedro basin (arizona/sonora). Journal of Hydrology 347, 48–66.

Solari, L., Van Oorschot, M., Belletti, B., Hendriks, D., Rinaldi, M., Vargas-Luna, A., 2016. Advances on modelling riparian vegetation-hydromorphology interactions. River Research and Applications 32, 164–178.

Tanaka, T., Tachikawa, Y., Ichikawa, Y., Yorozu, K., 2017. Impact assessment of upstream flooding on extreme flood frequency analysis by incorporating a flood-inundation model for flood risk assessment. Journal of hydrology 554, 370–382.

Tealdi, S., Camporeale, C., Ridolfi, L., 2011. Modeling the impact of river damming on riparian vegetation. Journal of Hydrology 396, 302–312.

Todorovic, P., 1970. On some problems involving random number of random variables. The Annals of Mathematical Statistics 41, 1059–1063.

Todorovic, P., 1978. Stochastic models of floods. Water Resources Research 14, 345–356.

Wong, M., Parker, G., 2006. Reanalysis and correction of bed-load relation of Meyer-Peter and Müller using their own database. Journal of Hydraulic Engineering 132, 1159–1168.

Zelenhasic, E.F., 1970. Theoretical probability distributions for flood peaks. Hydrology papers (Colorado State University); no. 42 .

Zen, S., Mueller, E., Hadden, R., Perona, P., 2018. Effects of stochasticity on rate of spread and fire front evolution statistics.

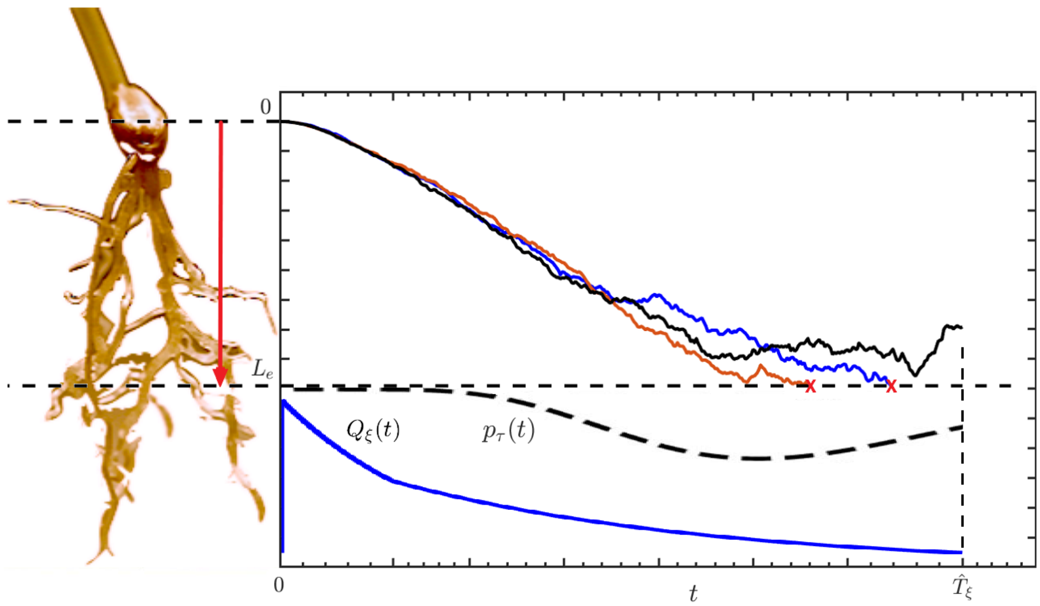

Figure 1: Illustration of the approach described by Eq. (2). The erosion rate evolves driven by flow hydrograph $Q_\xi(t)$, lasting $\hat{T}_\xi$, and erosion noise, g_t, so that different scouring trajectories result to a probabilistic distribution function, p_τ, of the times to uprooting. Vegetation is removed when total erosion reaches the critical erosion depth, L_e.

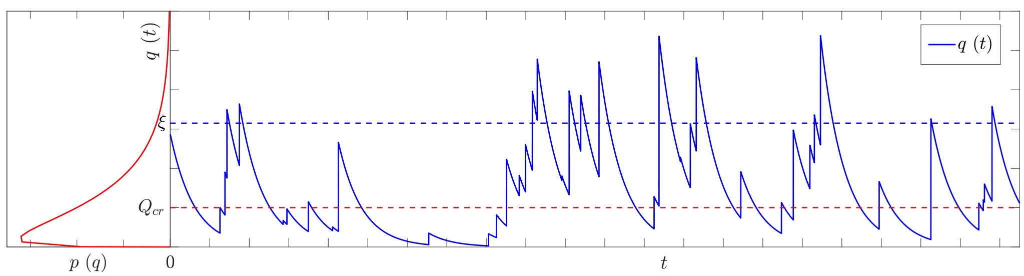

Figure 2: A sample realization of a Compound Poisson Process of flow discharge $q(t)$ (continuous blue line). Dashed blue line is the threshold ξ for extreme value analysis. Dashed red line is the critical threshold Q_{cr} for bed erosion. On the left the probabilistic distribution function $p(q)$ of flow discharge (continuous red line).

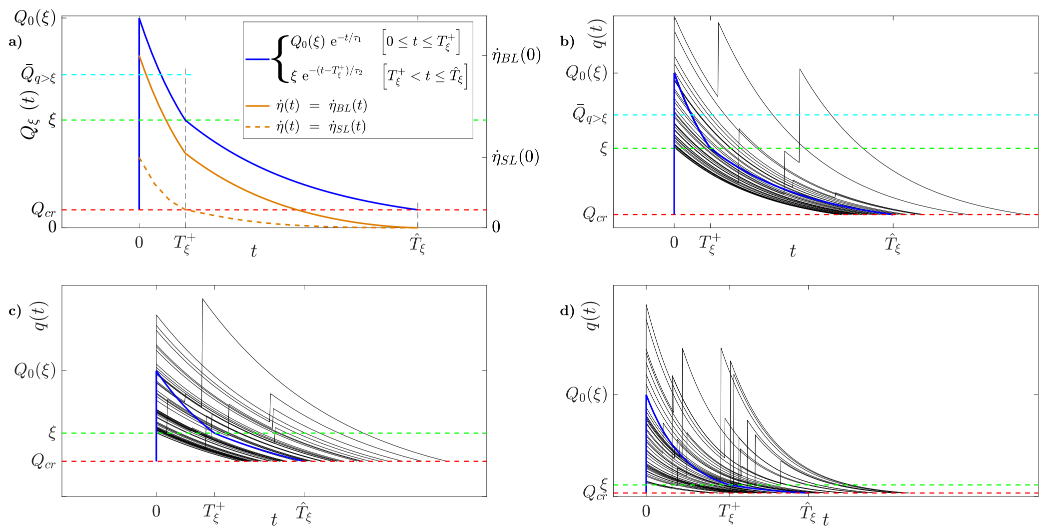

Figure 3: The reference mean event $Q_\xi(t)$ is the statistically averaged hydrograph associated to jumps above the threshold ξ. a) The reference mean event (continuous blue line) and its associated erosion rate, both in case of bedload (continuous dark-yellow line) and suspended load (dashed dark-yellow line) (see section 2.4). b) A comparison between the calculated hydrograph and some events above the threshold ξ extracted from a Compound Poisson Process. c) The reference mean event for the Small River whit ξ=180m^3 s^{-1} and some events taken from the CPP above such threshold. d) The reference mean event for the Large River with ξ=550m^3 s^{-1} and comparison to some events taken from the CPP.

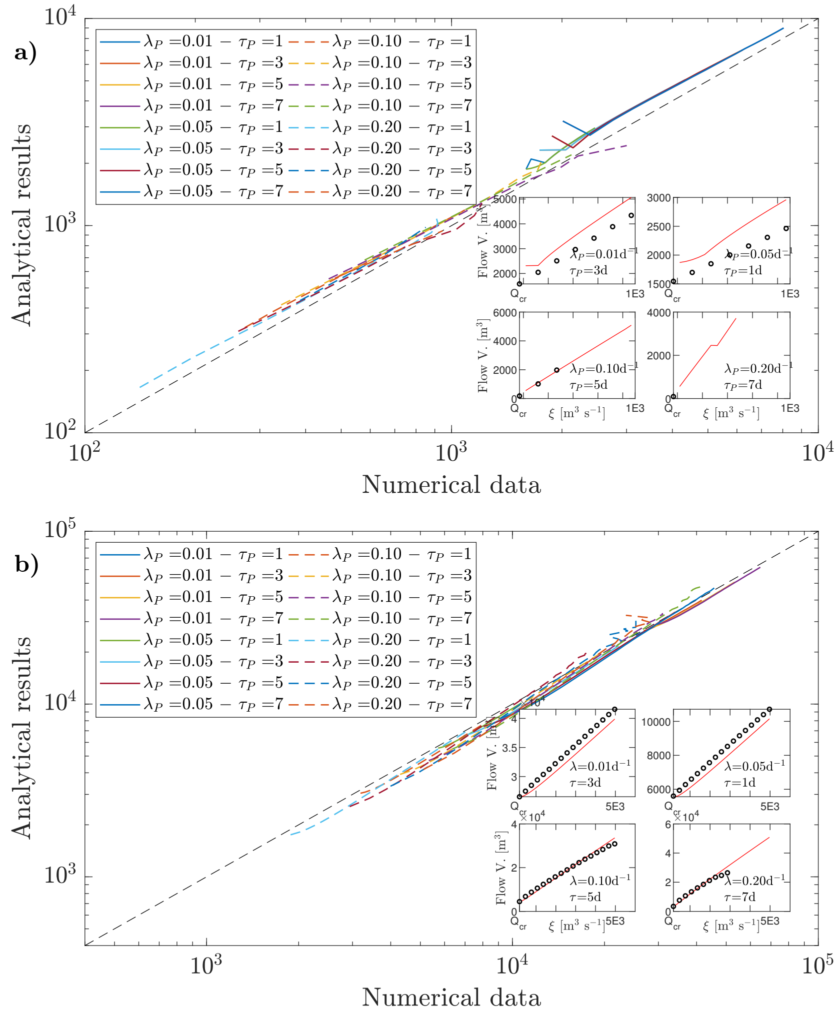

Figure 4: The flow volume comparison between the reference mean event (analytical results) and some events taken from the CPP (numerical data) for the two ideal rivers involved in the analysis. Values are in m^3. a) The comparison for the Small River. b) The comparison for the Large River. Inset panels show the agreement for different combinations of the parameters λ_P and τ_P, according to different values of the threshold ξ.

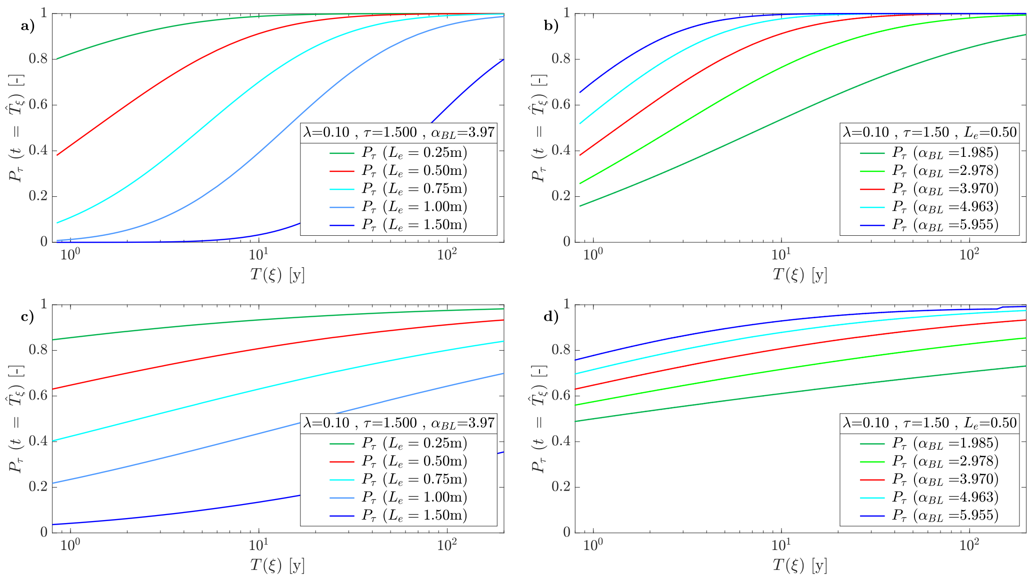

Figure 5: The uprooting probability, $P_\tau(t)$, in the Small River (panels a) and b)) and the Large River (panels c) and d)), at the end of the reference mean event ($t = \hat{T}_\xi$), according to different values of the parameters involved in Eq. (5). Values of the parameters are shown and, when not explicitly written, units are: [m] for L_e, [d^{-1}] for λ_P, and [d] for τ_P. a) and c) $P_\tau(t = \hat{T}_\xi)$ versus return period $T(\xi)$ varying the critical length of erosion L_e, for the Small River and the Large River, respectively; b) and d) $P_\tau(t = \hat{T}_\xi)$ versus return period $T(\xi)$ varying the coefficient α_{BL} in the bedload transport formula, for the Small River and the Large River, respectively.

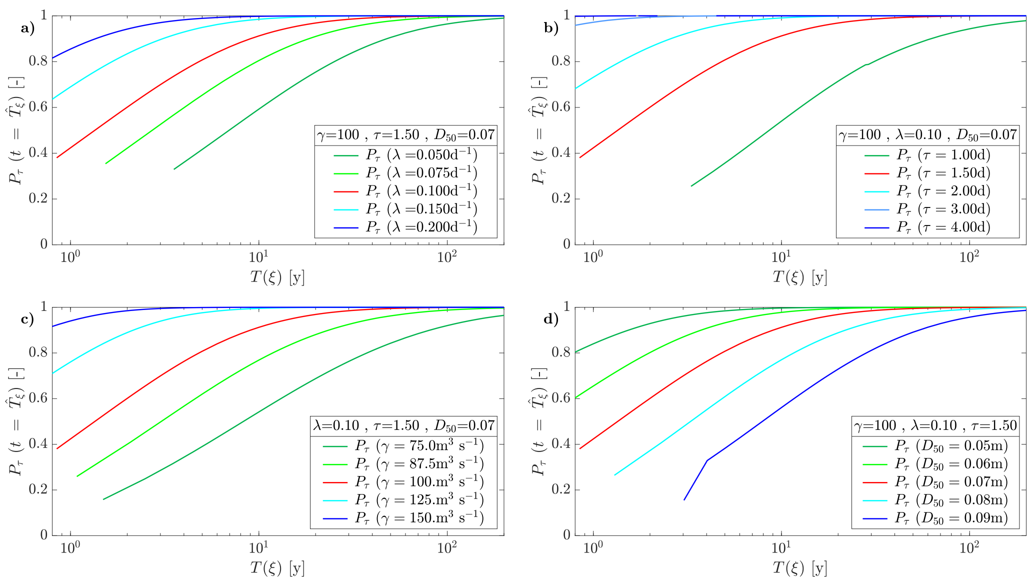

Figure 6: The uprooting probability, $P_\tau(t)$, in the Small River, at the end of the reference mean event ($t = \hat{T}_\xi$), according to different values of the parameters involved in Eq. (5). Noise in erosion process g_t is set to $0.05\text{m}^2\,\text{d}^{-1}$, values of the other constant parameters are shown. When not explicitly written, units are: [m] for L_e, [d^{-1}] for λ_P, and [d] for τ_P. a) $P_\tau(t = \hat{T}_\xi)$ versus return period $T(\xi)$ varying the mean frequency of jumps λ_P; b) $P_\tau(t = \hat{T}_\xi)$ versus return period $T(\xi)$ varying the exponential decay rate τ_P; c) $P_\tau(t = \hat{T}_\xi)$ versus return period $T(\xi)$ varying the mean jump value γ_P; d) $P_\tau(t = \hat{T}_\xi)$ versus return period $T(\xi)$ varying the mean grain size D_{50}.

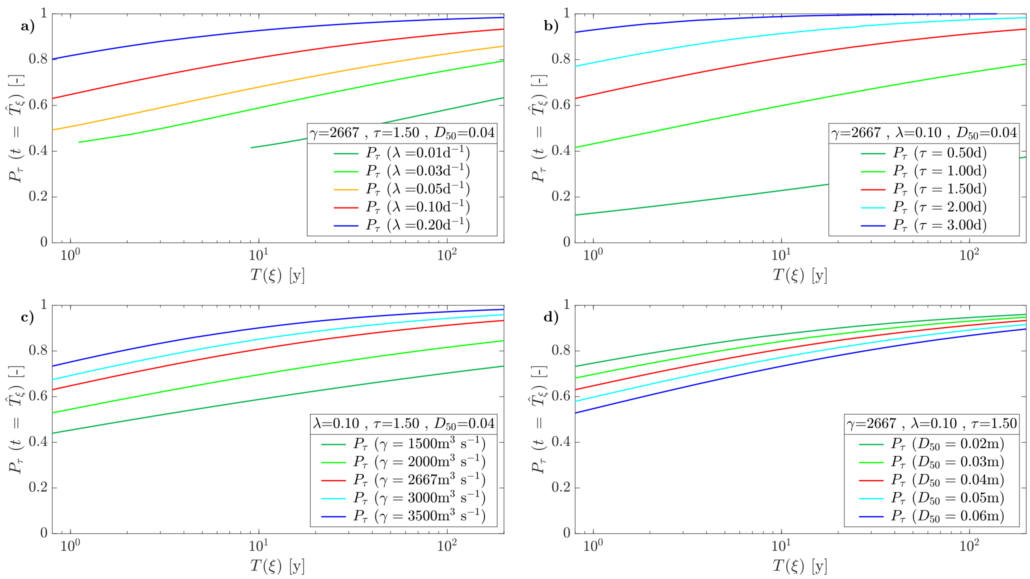

Figure 7: The uprooting probability, $P_\tau(t)$, in the Large River, at the end of the reference mean event ($t = \hat{T}_\xi$), according to different values of the parameters involved in Eq. (5). Noise in erosion process g_t is set to $0.05\text{m}^2\,\text{d}^{-1}$, values of the other constant parameters are shown. When not explicitly written, units are: [m] for L_e, [d^{-1}] for λ_P, and [d] for τ_P. a) $P_\tau(t = \hat{T}_\xi)$ versus return period $T(\xi)$ varying the mean frequency of jumps λ_P; b) $P_\tau(t = \hat{T}_\xi)$ versus return period $T(\xi)$ varying the exponential decay rate τ_P; c) $P_\tau(t = \hat{T}_\xi)$ versus return period $T(\xi)$ varying the mean jump value γ_P; d) $P_\tau(t = \hat{T}_\xi)$ versus return period $T(\xi)$ varying the mean grain size D_{50}.

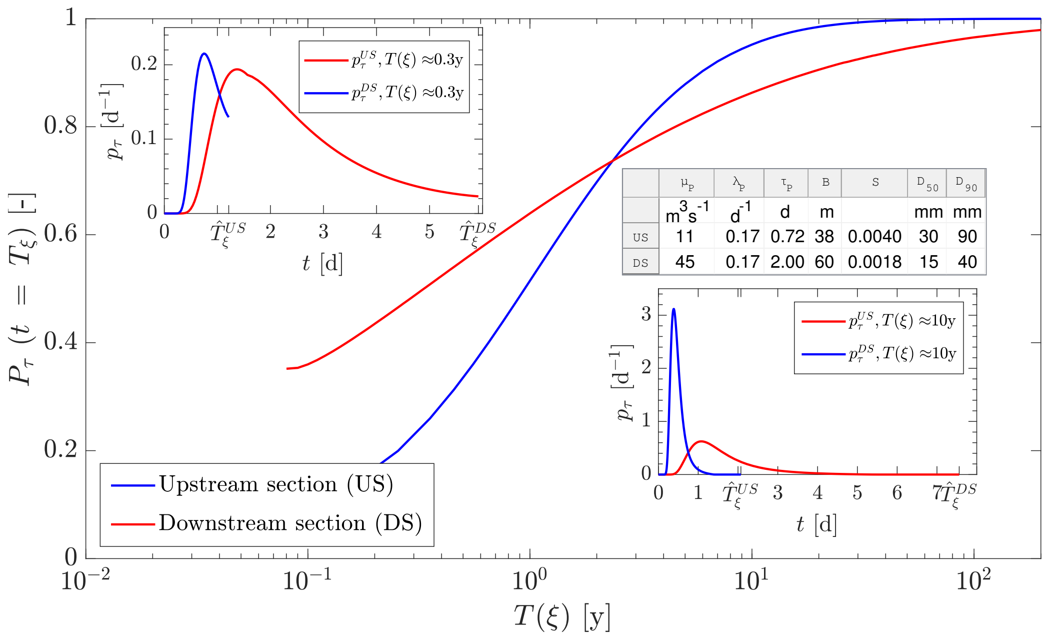

Figure 8: The uprooting probability, $P_\tau(t)$, at varying cross section. Hydro-morphological parameters are reported in the inset table. Blue line is for the upstream cross section (US), red line for the downstream one (DS). Inset panels show the probability distributions functions, p_τ, for short (e.g., $T(\xi)\ \approx$0.3y) and long (e.g., $T(\xi)\ \approx$10y) return periods.

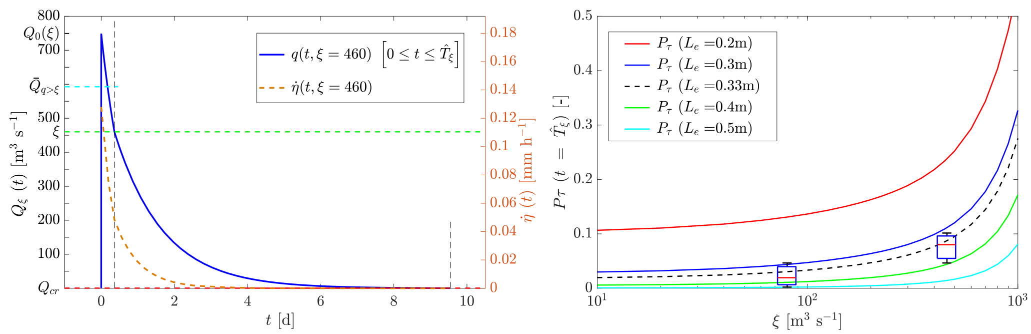

Figure 9: The uprooting probability $P_\tau(t)$ in the Santa Maria River, Arizona (USA) and comparison to the data calculated by Bywater-Reyes et al. (2015). a) The reference mean event $Q_\xi(t)$ for 10y return period and its associated erosion rate $\dot{\eta}_{SL}(t)$ due to suspended load. b) Comparison of $P_\tau(t = \hat{T}_\xi)$ with different L_e. Boxplots are the probability of uprooting calculated with measured data by Bywater-Reyes et al. (2015) for 2 and 10y return periods.

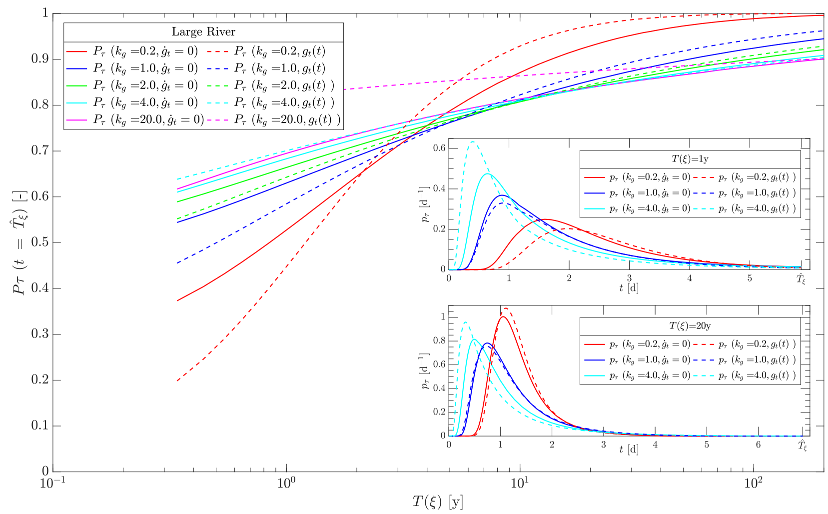

Figure 10: Graphical comparison of uprooting probability $P_\tau(t = \hat{T}_\xi)$ versus return period $T(\xi)$ for different values of the time-varying noise $g_t(t)$ (Eq. (3)) and its integral mean over the duration $\hat{T}_\xi$ for different values of the coefficient k_g of the *sediment mixing length* l_s (Eq. (4)) in the Large River. Continuous lines are for the uprooting probability with constant g_t, dashed lines are for the uprooting probability with time-varying g_t. In the inset panels the probability distribution functions, p_τ, corresponding to the reference mean event of two different return period (i.e., $T(\xi) = 1$y and $T(\xi) = 20$y) for different values of the coefficient k_g.